Article:

Abduraxman, B., Hubbard, P. orcid.org/0000-0003-2730-2538, Harrison, T. et al. (4 more authors) (2024) Acceleration-based friction coefficient estimation of a rail vehicle using feedforward NN: validation with track measurements. Vehicle System Dynamics, 62 (12). pp. 3235-3254. ISSN 0042-3114

https://doi.org/10.1080/00423114.2024.2323600

Vehicle System Dynamics
International Journal of Vehicle Mechanics and Mobility

ISSN: (Print) (Online) Journal homepage: www.tandfonline.com/journals/nvsd20

Acceleration-based friction coefficient estimation of a rail vehicle using feedforward NN: validation with track measurements

Bilal Abduraxman, Peter Hubbard, Tim Harrison, Christopher Ward, David Fletcher, Roger Lewis & Ben White

VEHICLE SYSTEM DYNAMICS
https://doi.org/10.1080/00423114.2024.2323600

Acceleration-based friction coefficient estimation of a rail vehicle using feedforward NN: validation with track measurements

Bilal Abduraxman[a], Peter Hubbard [a], Tim Harrison[a], Christopher Ward[a], David Fletcher[b], Roger Lewis[b] and Ben White[b]

[a]Wolfson School of Mechanical, Electrical, and Manufacturing Engineering, Loughborough University, Loughborough, UK; [b]The Department of Mechanical Engineering, The University of Sheffield, Sheffield, UK

ABSTRACT
Low friction can lead to poor adhesion conditions between the rail and wheel, which is detrimental to rail vehicle operation and safety. Up to date knowledge of the rail-wheel friction level is currently not available across rail networks, meaning planning mitigation strategies is difficult. This paper presents a real-time friction coefficient estimation algorithm based on a feed-forward neural network (FNN). Unlike conventional methods, the FNN does not depend on slip/adhesion curves or creep force models, and only requires wheelset longitudinal acceleration and speed. The wheelset acceleration and friction measurements are obtained by running a two-car rail vehicle on a friction-modified track with five different levels of friction conditions at four different vehicle speeds. Four different FNNs are trained for four speed conditions, and their estimation performance were validated by training multiple FNNs and testing them in each speed case using new sets of data. Validation results show that the average mean absolute errors from the four FNNs remains below 0.0083.

ARTICLE HISTORY
Received 29 September 2023
Revised 15 February 2024
Accepted 21 February 2024

KEYWORDS
Low adhesion detection; friction coefficient estimation; slip; creep; railhead conditioning

Introduction

Low adhesion conditions can occur due to track contamination such as wet-rail or compressed leaves that result in insufficient friction at the rail-wheel contact and create critical safety and operational issues. They can cause wheel spin/slide that can lead to network wide disruption due to defensive driving [1]. Poor adhesion conditions cost the UK rail industry and a wider public an estimated £355M each autumn [2]. It is a barrier to increasing capacity due to impact on the reliability and predictability of stopping trains under various adhesion conditions in a busy railway [2]. These problems show the importance of knowing accurate adhesion levels during operation so that their adverse effects can be mitigated [3]. The higher the acceleration/braking forces requirements, the higher the adhesion level

CONTACT Peter Hubbard p.d.hubbard3@lboro.ac.uk
*Christopher Ward has changed his affiliation recently to RAIB, Derby UK.

required. While overestimation of the adhesion levels can lead to unexpected longer braking distance that can increase risk of collision and derailment [4], underestimation can lead to unnecessary implementation of defensive driving.

Similar to the friction coefficient, the adhesion/traction coefficient is normally defined as the ratio between the reactive tangential force from the rail to wheel F_c and wheelset load Q. Since the reactive traction force F_c almost entirely originates from the wheel-rail friction force F_f [6] according to Newton's 3rd Law, and the wheelset load Q is approximately equal to the normal load from the rail to the wheelset N [5], maximum μ_a is usually equal to maximum kinetic friction coefficient μ [6], which is:

$$\mu_{amax} = \frac{F_{cmax}}{Q} \approx \frac{F_{fmax}}{N} = \mu \tag{1}$$

where μ_{amax}, F_{cmax}, and F_{fmax} are the maxima of μ_a, F_c, and F_f, respectively. Therefore, estimation of the friction coefficient can directly provide the estimation of maximum adhesion coefficient μ_{amax}, this being the crucial safety limiting value of relevance to a wheel slip or slide The adhesion coefficient depends on a number of factors due to the complex and nonlinear interaction between the rail and wheel that include wheel and rail geometries, track irregularities, and variable load distribution on a small contact patch area [7], while also being affected by external factors such as weather conditions [8] and contact surface temperature [9]. These factors make adhesion estimation a challenging and complex task [5], and accurate modelling of the wheel-rail contact is essential in studying the wheel-rail interactions and vehicle behaviour.

Adhesion estimation methods can be grouped into model-based and model-free approaches. Since it is difficult to directly measure or estimate the friction coefficient, most adhesion estimation methods rely on the estimation of the contact or creep forces, and slip/creepage that can indicate the adhesion level. Model-based methods are dependent on some prior knowledge about the vehicle model parameters when building a dynamic model to estimate the contact or creep forces, where those forces are then used to estimate the adhesion level [5]. These approaches include either a single wheel model [10], twin disc rolling contact test machines that can also be simulated by single wheel models [11–15], or wheelset models [16]. Authors in [17] used the ratio of the tangential to normal force to estimate the static friction coefficient using a roller rig. Nevertheless, rolling twin discs cannot incorporate the bogie/carbody motions that can affect the wheelset dynamics, such as changing the vertical wheelset load through coupling in the suspension forces. Although some methods also employ bogie or half vehicle models, as in [18,19], they still cannot inherently incorporate the full effect of bogie and carbody motions. This leads to full vehicle multibody models that can incorporate the full effects of carbody and bogie motion on the wheelset dynamics for better estimation of adhesion levels [20]. An innovative wheel-rail contact model was developed in [21] to reproduce accurate degraded adhesion conditions, and the model was also validated by experimental data measured from an instrumented Trenitalia one-car two-bogie vehicle driven on a degraded adhesion condition. In [22,23], measurements of vehicle body responses were used to estimate the contact forces. However, the high-frequency wheel-rail contact forces are low-pass filtered through the primary and secondary suspensions when they arrive at the wagon/vehicle body [22], and it is difficult to validate these contact force estimations without wheel-rail level contact force measurements [23].

Kalman filter (KF) or Kalman-Bucy filter (KBF) based adhesion estimation methods are generally model-based since they depend on some prior knowledge of the vehicle or contact force model parameters. Examples of extended KFs (EKFs) or unscented KFs (UKFs) used for adhesion estimation are given in [24–26]. A joint-UKF without post-processing was used in [27] to estimate the friction coefficient, where it requires at least 10 s of incoming data to reasonably estimate step changes in the friction levels. KBFs were also developed in [28–34] to estimate the creep/contact forces, and in [28–30] these forces were used to estimate the adhesion levels. The estimated creep forces and adhesion levels were validated in VAMPIRE simulation, but the adhesion estimation also introduces 5 s of delay that can have impact on operational implementation of the algorithm. In [35], residuals from multiple KF estimates of wheelset lateral and yaw states were fed to a fuzzy-logic system to estimate the adhesion condition. A non-linear estimator was developed in [36] for real-time estimation of the contact forces at different adhesion levels. The adhesion condition was estimated using only slip and tractive force in [37] without creep force models. An online observer to estimate the adhesion condition was also reported and compared to existing approaches in [38].

Artificial neural networks (ANNs) are model-free methods if they do not require any prior knowledge of the vehicle or the creep force models. ANNs have proven to be a valid alternative in solving rail-wheel contact problems with better computational efficiencies compared to classical approaches either when estimating the contact forces [39] or determining wheel-rail contact points [40], providing real-time performances similar to lookup tables [41]. The first example of using NN to estimate the adhesion was reported in [10], where a recurrent NN (RNN) provided a good and better estimation than a conventional method. A feedforward NN (FNN) was trained and validated in [42] with experimental measurements of vehicle speed, wheelset angular speed, and brake pressure to accurately estimate the adhesion levels from slip curves. An FNN is also implemented as part of a kernel extreme learning machine with radial basis function (RBF) and particle swarm optimization (PSO) to estimate stable and unstable regions of adhesion in [43], rather than adhesion levels. PSO was also used in [44] to estimate and experimentally validate the adhesion coefficients for dry and wet conditions.

Most of the above mentioned research depends on slip for estimation of adhesion levels. Nevertheless, slip requires accurate knowledge of wheelset speeds that are not always available on vehicles, which lack an independent land based datum point, or high-resolution instrumentation on the wheel. Although the authors in this paper had access to the encoder signals from the WSP system, slip is subject to drift since longitudinal wheelset velocity in most cases is only obtainable by integrating wheelset acceleration. Therefore, drift-free slip is not easily available. In addition, the conventional slip/adhesion curve is very steep at low levels of slip/creepage, which makes the precision of slip more important to such estimators and these estimators will always be sensitive to low levels of slip measurements, requiring the occurrence of larger slips for accurate estimation of adhesion levels. However, large slips only happen during wheel spin or slide during braking instances, which can impact the accuracy of slip-based estimators in normal running conditions without braking or wheel spin. Arguably any estimation which requires a large slip before it can be calculated is inherently going to be too late to be of value.

Furthermore, none of the methods above solely employ wheelset accelerations, or wheelset acceleration/speed from a full-size vehicle without braking for estimating adhesion/friction levels. In this paper, an accurate estimation of friction coefficient is realised through an FNN that is trained and validated by friction and wheelset acceleration measurements obtained from a full-size test vehicle on a friction-modified track. Water, paper-based tape, and standard top-of-rail products are applied to the rail head to achieve five different friction conditions including low friction. Vehicle body, bogies and wheelsets are all instrumented with accelerometers and potentiometers for taking measurements when the rail vehicle goes over the friction modified track. The FNN friction estimation algorithm is only based on wheelset acceleration measurements, and does not depend on slip/adhesion curve, creep force models, or braking commands as in [21,42]. It is also more accurate than swam intelligence based static friction coefficient estimator in [43], which was validated by experimental data from roller disc tests. Four different FNNs are trained for four different constant speed conditions and their estimation performance for the validation data are presented.

Slip dynamics

Since slip/creepage during normal operation without braking or wheel sliding is quite small, the slip dynamics is analysed first. Slip arises from both deformation and sliding instances at the wheel-rail contact due to instances of friction force saturation. Longitudinal slip s_x is proportional to the difference between the circumferential wheelset velocity ωr_w and the translational inertial wheelset velocity in the longitudinal direction $\dot{x}_w$, where ω is the wheelset rotational speed, and r_w is the wheel radius. It is also referred as slip ratio and is commonly given by:

$$s_x = \frac{\dot{x}_w - \omega r_w}{\dot{x}_w} \tag{2}$$

where $\dot{x}_w - \omega r_w$ can be referred as longitudinal slip velocity. It can be seen in this equation that any velocity difference between $\dot{x}_w$ and ωr_w can create a non-zero slip. A positive slip occurs when $\dot{x}_w > \omega r_w$, which can be referred to as a translational slip (including braking slip), and a negative slip when $\dot{x}_w < \omega r_w$, which can be referred to a as spin or accelerating slip. Note that since there can be non-zero slip instances without braking, we have introduced a more inclusive term 'translational slip' instead of just using 'braking slip'. If $\dot{x}_w$ and ωr_w are equal, then slip is zero. Slip can only be zero or near zero when the leading and trailing parts of the deformation at the contact patch are symmetrical so that although the wheel is rolling there is no velocity difference between $\dot{x}_w$ and ωr_w. This can also happen when the vehicle is at rest so that the wheel-rail deformations are symmetrical. Friction and consequent adhesion can also be dependent on the vehicle speed rather than just slip [46]. However, existing slip/adhesion curves all show that the creep/adhesion forces are zero for zero slip [45].

The dynamics of slip can be explained by the slip dynamics/rate, which can be obtained by the rate of change of slip. The longitudinal slip dynamics is then given by time-differentiating eq. (2), which is given as follows when r_w is assumed constant:

$$\dot{s}_x = \frac{\ddot{x}_w \omega r_w - \dot{x}_w \dot{\omega} r_w}{\dot{x}_w^2} \approx \frac{\dot{x}_w\left(\ddot{x}_w - \dot{\omega} r_w\right)}{\dot{x}_w^2} = \frac{\ddot{x}_w - \dot{\omega} r_w}{\dot{x}_w} \tag{3}$$

Figure 1. MPV with instrumented car nearest the camera.

where $\omega r_w \approx \dot{x}_w$ when the slip velocity is small. This equation shows that $\dot{s}_x \propto \ddot{x}_w - \dot{\omega} r_w$, which means measurements of $\ddot{x}_w$ and $\dot{\omega}$ can indicate the amount of slip rate since r_w is fairly constant. $\dot{s}_x$ will be larger when the difference term $\ddot{x}_w - \dot{\omega} r_w$ is larger, and $\ddot{x}_w - \dot{\omega} r_w$ can become larger when there are contact saturations that will either cause translational or spin slip instances. This is because contact saturations can also cause changes either in $\ddot{x}_w$ or $\dot{\omega} r_w$. This means that saturation events can lead to increased $\dot{s}_x$. Since higher or frequent saturation instances happen more often when μ is low (according to Coulomb's law), then it follows that there is an inverse relationship between $\dot{s}_x$ and μ. The value of μ can affect the wheelset behaviour that manifests in both $\ddot{x}_w$ and $\dot{\omega}$, and in this paper, we have investigated if it is possible to estimate μ only using $\ddot{x}_w$ as input to the NN. Essentially, the NN finds a functional relationship between $\ddot{x}_w$ and μ. It is not dependent on Eq. (3), and Eq. (3) is analysed to provide some theoretical basis as to why the NN friction estimation might work with acceleration inputs only. Even if there is a large slip velocity such that $\omega r_w \neq \dot{x}_w$, $\dot{s}_x$ is still proportional to both $\ddot{x}_w$ and $\dot{\omega}$ Eq. (3).

Instrumentation and testing

Instrumentation

The test vehicle used is a multi-purpose vehicle (MPV) owned by Network Rail that comprises of two cars each with a pair of four-wheel bogies. Only one of the cars is instrumented, and it is shown in Figure 1 below.

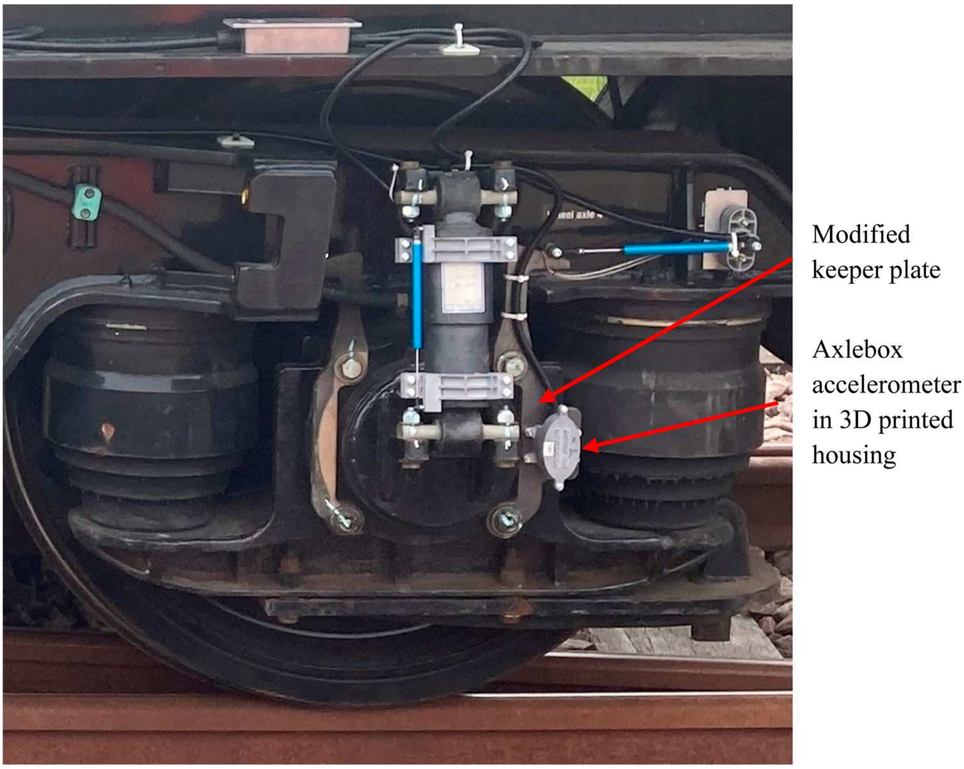

Figure 2. One of the eight axlebox accelerometers fitted on a modified keeper plate.

Instrumentation of the vehicle was carried out by Perpetuum owned by Hitachi Rail who has experience of instrumenting in-service trains. The vehicle was instrumented by accelerometers and potentiometers on all four wheelsets and two bogies. The left and right axleboxes of the wheelsets were instrumented with 3-axis Dytran 7533A4 accelerometers. They were fitted on the axlebox on a modified keeper plate in a 3D printed housing (Figure 2).

The data acquisition system used a National Instruments cDAQ-9185 chassis, and an industrial computer in the front enclosure recording onto a solid-state hard disk. Data was sampled at 5120 Hz.

Testing and railhead conditioning

Testing was undertaken at Network Rail's Tuxford rail innovation and development centre [47]. A 400-m section of straight and generally level track was identified as a test section. The test runs were always completed in the same direction, with the instrumented car leading. The train was run through the test section at different speeds and over artificially created low adhesion conditions at constant speeds of 16mph, 26mph, 40mph and 60mph.

In addition to the dry condition, the railhead at the test section of the track was prepared with four different friction methods to create different friction conditions. Spray equipment was fitted to the vehicle, with water containers and pumps on the vehicle bed

Table 1. Rail head friction modification conditions.

Condition	C Surface Modification	Application method	Expected friction coefficient range
Dry	None	N/A	0.4–0.5
Friction Modifier	Water based friction modifier	Paint roller (by hand)	0.25–0.4
Wet	Water spray	On-train spray equipment	0.15–0.3
Detergent	5% detergent in water	On-train spray equipment	0.1–0.15
Paper tape	Wetted paper tape	On track hand trolley – wetted using an on-train spray equipment	0.1 or lower

Table 2. Friction levels achieved on the straight section of the test track.

Condition	Dry	Friction modifier	Wet	Detergent	Paper tape
16 mph	0.31	0.14, 0.17	0.161	0.18	0.16
26 mph	0.29	0.19	0.191	0.21	0.16, 0.22
40 mph	0.31, 0.37	0.17	0.24	0.22	0.1
60 mph	0.3, 0.35	0.16	0.27	0.24	0.11

applying liquid to the rail head immediately ahead of the leading wheels. Details of the friction conditions achieved are described in Table 1 below.

The wet and 5% detergent conditions used a water spray equipment designed and fitted on the vehicle, where premixed detergent/water was supplied to a spray ahead of the wheels on both rails at one end of the vehicle from in the containers on the vehicle deck. The friction modifier used was a commercially available product specifically designed to maintain a mid-range friction coefficient between wheel and rail.

Paper tape is an established industry method [48] used to create repeatable low friction. When the paper tape is mixed with water, it can form a hydrogel, previously reported to be a potential mechanism of low friction during leaf fall season [49]. To create a paper tape layer, a rail trolley equipped with two rolls of gummed paper tape was pushed down the test section (Figure 3). The trolley was fitted with on-board water sprays and rollers, which wet and press the tape onto the railhead. The MPV was then rolled over the tape section 3 times, with no further water spraying, to condition the tape layer.

Friction measurement

To assess the level of friction obtained, the OnTrak tribometer (Figure 4) was used for friction measurements. The OnTrak portable railhead tribometer can produce a range of slip and angle of attack between an instrumented wheel and the rail enabling more controllable contact conditions than a pendulum skid resistance tester that has been used extensively in railways as a simple method for railhead friction measurement [50,51].

After modifying the friction levels, the friction coefficients were measured immediately following the train passing at two points separated by 20 m and their average taken. This paper focuses on the data from the straight section of the test track, where six different friction-modified conditions per speed case are used in this study, and the friction measurements for each run are tabulated in Table 2.

From Table 2, it can be seen that the friction coefficients have some variations even for a same friction condition, reflecting the real-world as opposed to lab conditions in which wind, sun exposure, and in some paper-tape based tests rain, varied during the tests [52].

Figure 3. The tape laying trolley laying paper tape on the railhead.

Another effect that can add to the variations in the friction measurements could be the effect of passing of multiple wheels on the same section of the track [53]. This is referred as polishing effect and can introduce a difference between the friction coefficient measured before and after the vehicle passing. From the measurement perspective, the polishing effect becomes a part of the uncertainty between the actual friction experienced by the vehicle and the measured friction. Thus, polishing effect can become a part of measured friction.

Note that the measurements are taken up to 2 decimal places, but a value of 0.001 have been added to the wet conditions of 16 and 26 mph cases so that they can be differentiated both in the coding variables and later in the data labels. This is used to avoid using the same names for different tests because the same acceleration states in the code can only be

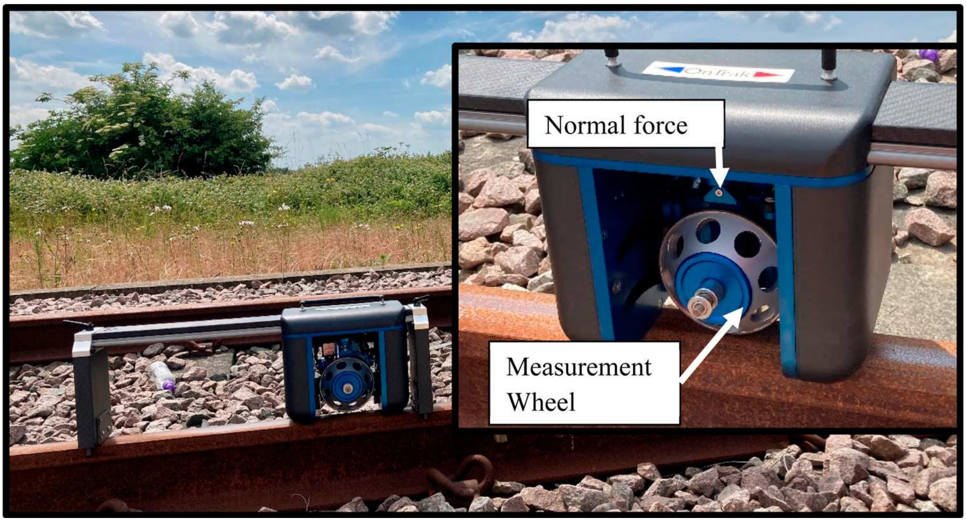

Figure 4. The OnTrak tribometer.

distinguished for different tests if they are named uniquely. This 0.001 only affects naming and labelling of the data and is not added to the actual friction values.

For test point listed in Table 2, all data from the sensors specified were recorded for off-line processing. Other details about the tests and procedures can be found in [52,54].

FNN estimation

By the universal approximation theorem, NNs can approximate any continuous function if it has at least one hidden layer and uses non-linear activation functions. It is decided to use FNNs because they are more stable and easier to train than RNNs.

Input selection

Good selection of NN inputs can greatly improve estimation accuracy without increasing size or complexity. Selection of NN inputs depend on the underlying physical relations between the inputs and the outputs. Ideally, a single NN should be trained for all speed conditions since vehicle speed is a continuous variable. However, this requires linking all the data from 24 test runs in Table 2 one after the other into a single input-output set of time-series data for training and validation. Due to the high sampling rate in the test data, the linked data requires hundreds of GBs of random-access memory (RAM) during training. Therefore, for the estimation study in this paper, four different FNNs representing four different speed conditions are trained and studied, where each FNN has six sets of input-output data linked together.

The motivation for using wheelset accelerations rather than slip or creep force is two-fold. First, as mentioned earlier, calculation of the slip or creep forces require accurate measurements of $\dot{x}_w$ and ω, where $\dot{x}_w$ is subject to drift when it is obtained from integrating $\ddot{x}_w$, which makes $\dot{x}_w$ and subsequently the slip s_x also subject to drift without a GPS or Doppler speed sensors at the wheelsets. It is also difficult to obtain ω without access to

WSP signals. Second, even if the slip is measured without drift, conventional slip/adhesion curves produce zero adhesion when the slip is zero and they require sufficient non-zero slip to generate the full adhesion curve, which usually only happens during braking that leads to large translational slip [42]. This is because slip/adhesion curve is commonly very steep in the beginning for small slip and only starts to become more distinct for different friction levels when there is sufficient slip, making y-axis adhesion estimation sensitive to very small slip/creepages in x-axis. These two reasons make using wheelset acceleration states $\ddot{x}_w$ and $\dot{\omega}$ more appealing than velocity states. Although $\dot{\omega}$ was measured using WSP system, this paper focuses on using $\ddot{x}_w$ for inferring the friction coefficient. It is already shown that $\ddot{x}_w$ have inverse relation with μ from the slip dynamics, and $\ddot{x}_w$ is also simpler to obtain drift-free compared to two velocities required to compute slip. In addition, accelerations are better suited to detect changes in motion since they can detect larger amplitudes in vibrating motion compared to velocities, i.e. acceleration signals have higher signal-to-noise ratio when detecting vibrations.

Although this paper focuses on mapping wheelset acceleration behaviour to friction levels, vehicle speed can significantly affect wheelset accelerations because higher vehicle speed means higher vehicle movement forces (cornering, response to track irregularities), and higher aerodynamic forces indirectly affecting the suspension systems, where both factors can increase the wheelset acceleration magnitudes and frequency through the increased suspension forces, as shown in the wheelset dynamics. This will also be shown by the wheelset acceleration data shortly. Therefore, vehicle speed plays an important role in the estimation algorithm. Nevertheless, since the vehicle speeds are constant when using four different FNNs, it is not an input at this stage.

There are three acceleration states that can be used for the NN at each axle: longitudinal, lateral and yaw accelerations. Yaw accelerations are obtained by the difference between right and left axlebox longitudinal accelerations. Initially, all three states from all four wheelsets were used as inputs. Although the NN is capable of building an estimator using accelerations from a single wheelset, investigations began by including all of the wheelsets with a hypothesis that a better NN estimator could be created because all four wheelsets can have unique behaviours at each friction levels due to the overall nonlinearities, non-symmetric mass distributions, and driven/undriven conditions of the wheelsets. For example, if one wheelset has a weaker relationship between its motion and μ at a certain friction condition, then other wheelsets may have stronger relationship with μ at this friction condition. In addition, using multiple sensors from multiple wheelsets also provide robustness to faults in individual sensors. After some initial training and validation studies it was found that not all of the wheelset accelerations are necessary to produce similar level of estimation performance, and that at least four states are necessary for good estimation.

Due to a large number of input states, input combinations are made by group combinations that are obtained by combining different DOFs of all wheelsets. The input combinations from all four wheelsets studied are: (1) 12 states of longitudinal, lateral, and yaw accelerations, (2) 8 states of longitudinal and lateral accelerations, (3) 8 states of longitudinal and yaw accelerations, (4) 8 states of lateral and yaw accelerations, (5) 8 states of longitudinal left and right accelerations, (6) 4 states of longitudinal accelerations, (7) 4 states of lateral accelerations, and (8) 4 states of yaw accelerations. After some training and validation studies using all of these different inputs, it was found that 4-state longitudinal or yaw accelerations can provide similar levels of estimation accuracy compared to using 8 acceleration states from longitudinal and yaw DOFs. In addition, longitudinal and/or yaw accelerations produce slightly better estimations compared to lateral accelerations. This can be explained by the wheelset dynamics where longitudinal accelerations vary more compared to lateral accelerations since lateral accelerations are mainly caused by vehicle guidance due to wheel conicity, and longitudinal slip is generally larger than lateral slip, making longitudinal slip and accelerations easier to detect. Therefore, the input layer of the FNN chosen here consists of four states of longitudinal accelerations from all wheelsets.

Data processing

The axlebox accelerometers have positive DC offsets at zero accelerations, which range from 266 to 272 m/s^2 after conversion from volts to m/s^2. In order to relate true acceleration amplitude to friction coefficient, the DC offsets are removed first by using a high-pass filter (HPF) with 0.0001 Hz cut-off frequency. The very low cut-off frequency of the HPF helps remove a significant drift in the data that have otherwise also led to drifts in the estimations.

The acceleration measurements also contain high-frequency noise, which is generally due to sensor noise and vehicle vibrations. However, it could also contain translational slip instances as shown by the slip dynamics. The reason for this is that changes in translational slip can be registered as an acceleration by the accelerometer in $\ddot{x}_w$, which leads to translational slip in (2). Even a small slip instance can be registered as high magnitude of $\ddot{x}_w$ if it happens in a very short period, which is the case here with a high sampling rate. This is shown by the slip dynamics given in (3), where $\dot{s}_x \propto \ddot{x}_w - \dot{\omega} r_w$.

The high frequency noise from the sensors can lead to fluctuating friction estimations, and thus, a low-pass filter (LPF) with 1 Hz of cut-off frequency is used to flatten the high frequency part of the data.

The high-pass and low-pass filtered signals also contain positive and negative amplitudes that are not necessarily equal. This can be due to the combination of overall vehicle condition, nonlinearities, keeper plate modes of vibration, conicity and any asymmetries in mass distribution and suspension parameters along each axis leading to asymmetric oscillations. Asymmetric oscillations can then result in asymmetric magnitudes in the positive and negative cycles of the wheelset accelerations. The asymmetric oscillations can also be skewed towards the direction of travel, and negatively dominant oscillations can become positively dominant when the train is travelling in the opposite direction. Therefore, in order to reduce the effect of asymmetries and direction of travel, absolute norms are applied to the filtered accelerations. The wheelset longitudinal accelerations after applying HPF, LPF and absolute norm are shown below from Figures 5–8, where $\ddot{x}_{wi}$ denote the processed longitudinal acceleration of the i-th wheelset.

Note that without the HPF, there is significant drift the data to the point that it can critically affect the FNN estimations. Figures 5–8 show that the HPF and LPF help remove the drift and render the acceleration data smooth. This is helpful for classification since smooth and drift-free data produce closely packed and separate clusters of acceleration data points in the acceleration vs friction level x-y plot. It can also be seen that higher speeds lead to larger acceleration amplitudes, as would be expected from increased accelerations in response to track imperfections, and higher influence of aerodynamic forces acting through the suspensions systems at higher speeds.

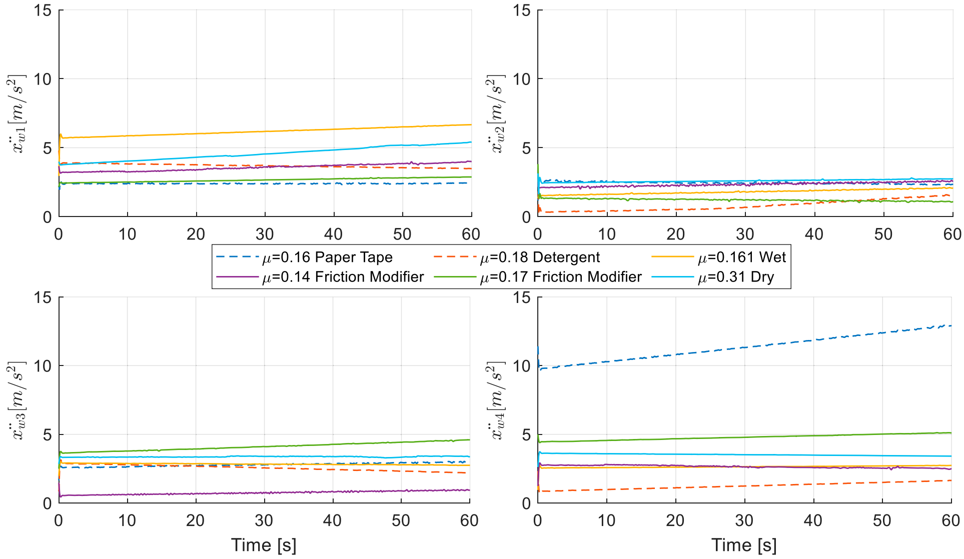

Figure 5. Wheelset longitudinal accelerations at 16 mph after HPF, LPF and absolute norm.

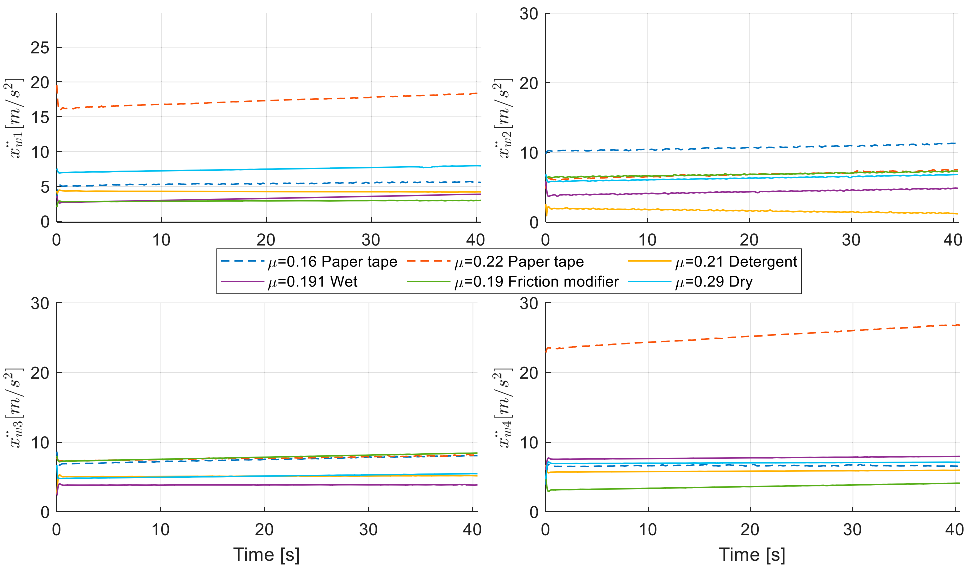

Figure 6. Wheelset longitudinal acceleration at 26 mph after HPF, LPF and absolute norm.

In addition to the HPF and LPF, the training data sets were down sampled using averaging by factors of 50, 100, 150, and 200 for 60, 40, 26 and 16 mph cases, respectively. This means that a single training data sample at 60 mph is an average of 50 nearby data samples from the original data. The reason for down sampling is to speed up the training process since there are significant amount of data due to the high sampling rate and longer periods, even when the data are trained separately at four different speeds, and the algorithm only focuses on the low frequency part of the data. This has almost no effect on the processed

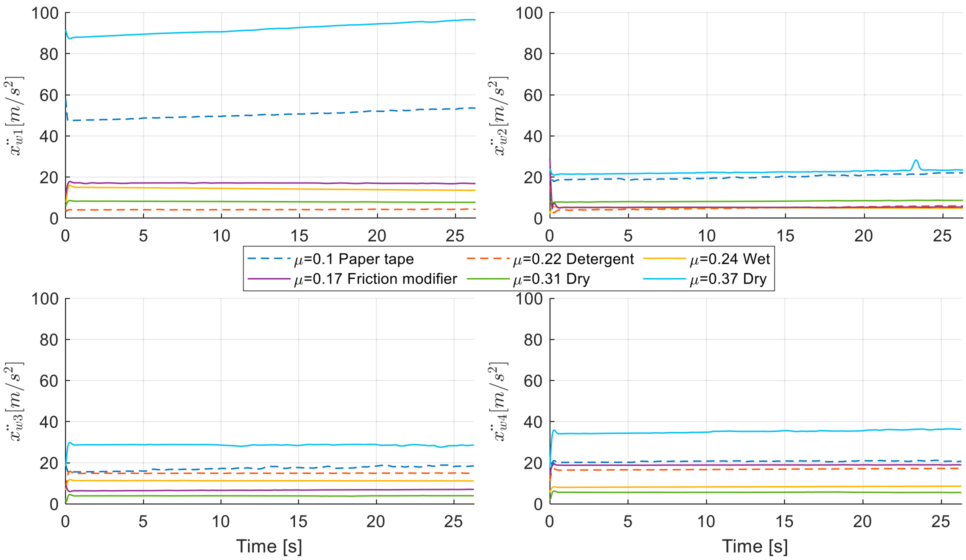

Figure 7. Wheelset longitudinal acceleration at 40 mph after HPF, LPF and absolute norm.

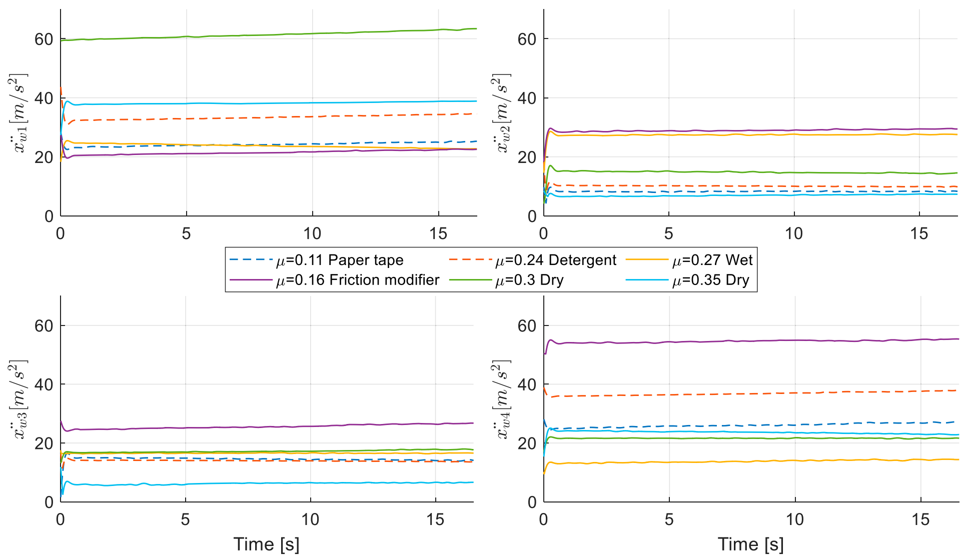

Figure 8. Wheelset longitudinal acceleration at 60 mph after HPF, LPF and absolute norm.

data since they are already made smooth by the HPF and LPF. Note that down-sampling is common in classification when there are large training data.

Lastly, the NN inputs are also pre-processed by normalising them to a range between [−1,1]. This was achieved by dividing inputs by their maximum and minimum values. Input normalisation improves NN training process, and has been beneficial in reducing minor fluctuations in the NN output since input acceleration magnitudes have some variations between the wheelsets as shown from Figures 5–8.

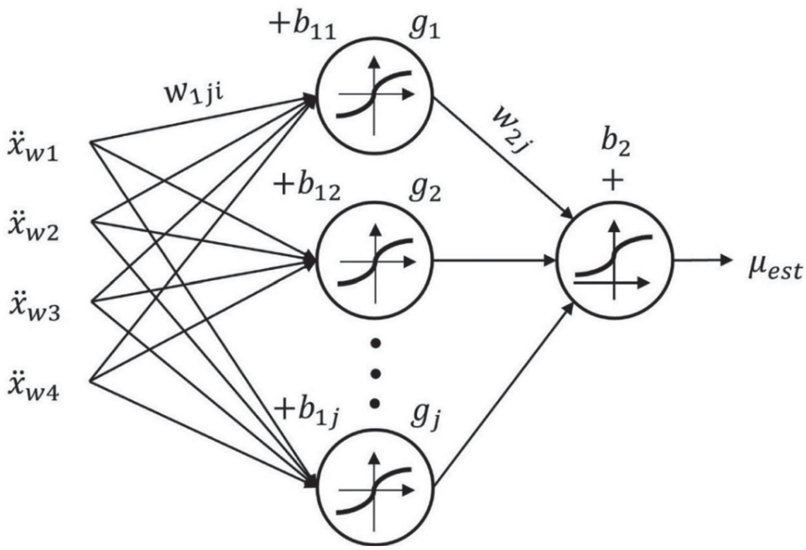

Figure 9. Structure of the FNN.

Estimation

The NN friction estimation problem is treated as pattern recognition (PR) rather than curve fitting because output layers of PR use activation functions with values between 0 and 1, rather than positive and negative values usually found in the regression functions for curve fitting. This type of activation function is more suitable for friction estimation because actual friction levels are also between 0 and 1 under any condition. The FNN structure is shown below in Figure 9.

In Figure 9, $\boldsymbol{x} = [\ddot{x}_{w1}, \ddot{x}_{w2}, \ddot{x}_{w3}, \ddot{x}_{w4}]^T$ denote the input vector of processed longitudinal wheelset accelerations with size $i = 4$, $\boldsymbol{w}_{1\boldsymbol{j}}$ is the j-th vector of j-by-i input weight matrix with j as the total number of hidden layer neurons, g_j is the output of j-th hidden layer neuron, w_{2j} and b_{1j} are the hidden layer weight and bias vectors with size j, respectively, b_2 is the output bias, and μ_{est} is the estimated friction coefficient. After multiple training and validation studies, it was found that around six hidden layer neurons provide the best estimation accuracy for all speed cases, which gives a maximum of six for j.

The NNs are trained using the first 80% of each test data in Figures 5–8, and the remaining 20% is used for validation. The FNN performance are assessed using the validation data set that the FNN have not seen before during training. During training, the processed acceleration inputs and actual measurements of μ are fed to the training process to optimise the NN parameters. During validation, the NN friction estimate is given by:

$$\mu_{est} = \frac{1}{1 + e^{-w_{2j}g_j}} + b_2 \tag{4}$$

$$g_j = \tanh(\boldsymbol{w}_{1\boldsymbol{j}}\boldsymbol{x} + b_{1j}) \tag{5}$$

where the hidden and output layer activation functions are hyperbolic tangent and logsig functions.

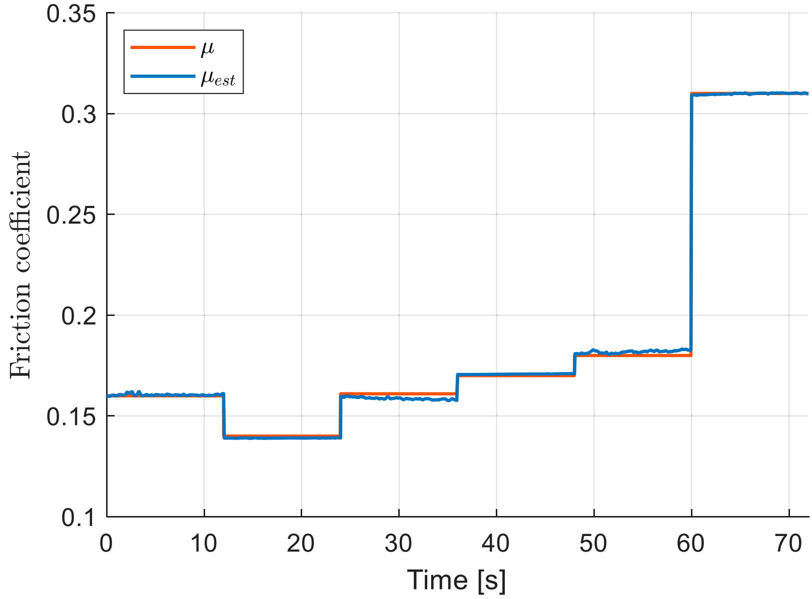

Figure 10. Estimation performance of the FNN at 16 mph.

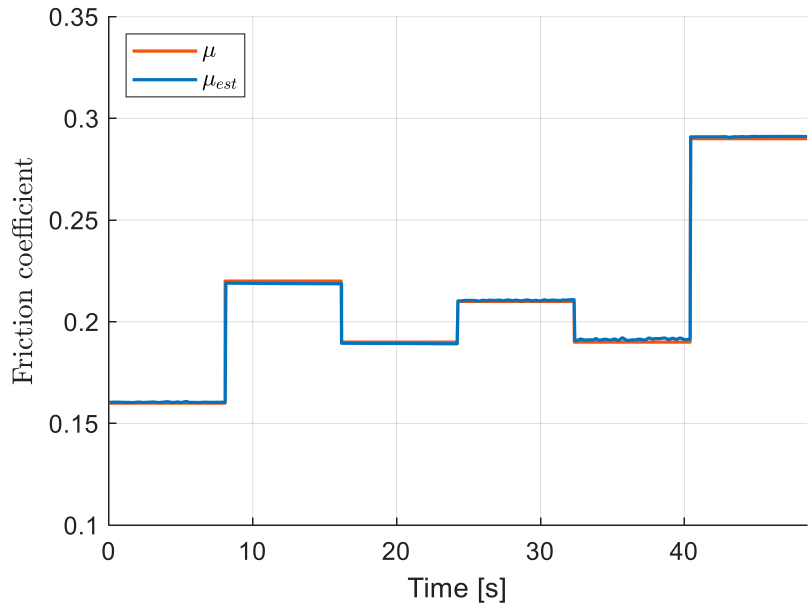

Figure 11. Estimation performance of the FNN at 26 mph.

The FNNs' estimation performances for the validation data set are shown in Figures 10–13. These are some of the best performing FNNs after training 15 FNNs for each speed case. Note that the discontinuities are due to linking different test runs into the same time axis. The mean absolute errors (MAEs) between the measured and estimated friction coefficients for these FNNs are 0.0011, 0.0009, 0.0021 and 0.0027, respectively.

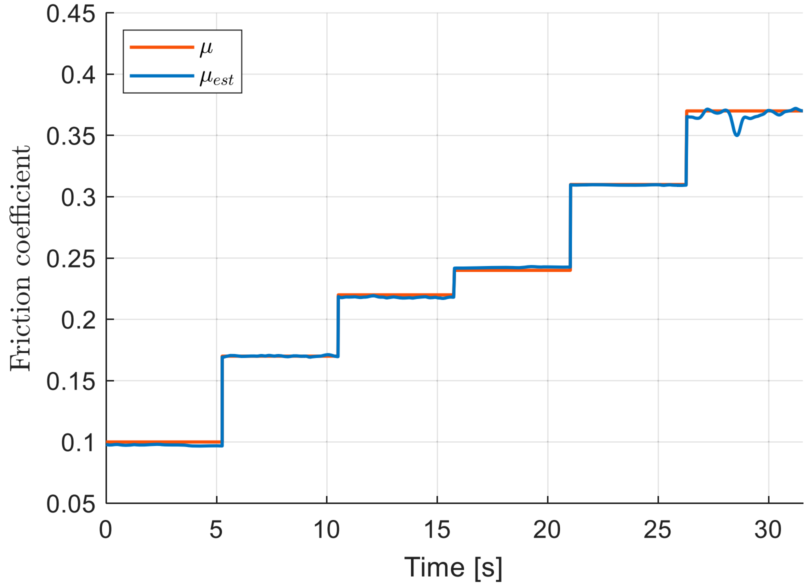

Figure 12. Estimation performance of the FNN at 40 mph.

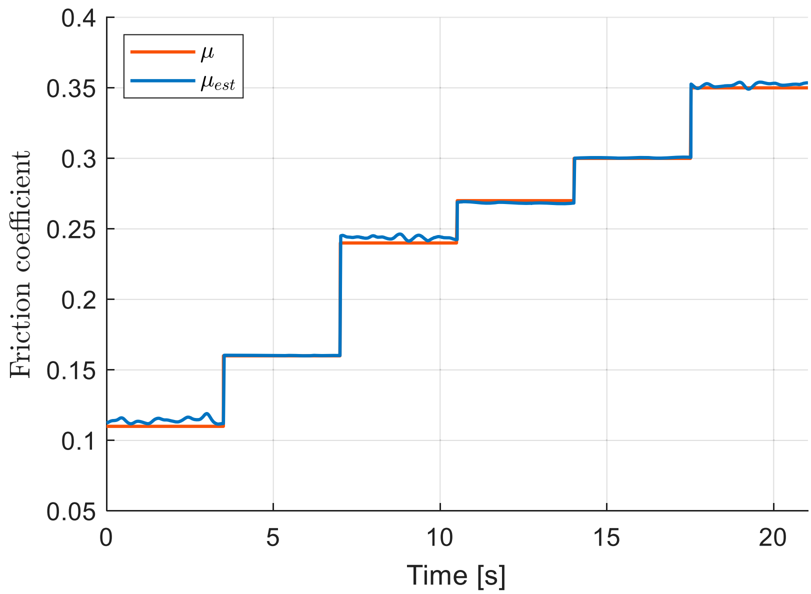

Figure 13. Estimation performance of the FNN at 60 mph.

The FNNs were trained and validated times because the weights and biases are initialised randomly in each training instance, and this random initialisation results in different optimal NNs after each training process. In order to reduce the effect of random initialisation on actual performance of the FNN, 15 FNNs were trained and validated for each speed case and both average RMSEs and average MAEs of 15 FNNs are tabulated in Table 3 below. It shows that the FNN performs better at lower speeds compared to higher speeds. This can

Table 3. Average RMSEs and MAEs of 15 FNNs trained and validated for each speed case.

Speed	16 mph	26 mph	40 mph	60 mph
Average RMSE	0.0053	0.0038	0.0141	0.008
Average MAE	0.0041	0.0028	0.0083	0.0063

be attributed to the fact that there is more structural vibration at higher speeds so that relatively less amount of wheelset accelerations is related to slip, compared to lower speeds cases where there are less structural vibrations and hence, more of the wheelset accelerations are related to slip. In addition, there are also longer training data available at lower speeds compared to higher speeds, which can also contribute the better training of the FNNs at lower speeds.

The FNN has a simple structure with only six neurons in a single hidden layer, which reduces the training and computational time when implementing. In terms of computation time, both the HPF and LPF are IIR filters, and therefore, it is possible to achieve a near real-time friction estimation, if not real-time, when this algorithm is implemented. However, further studies are needed before implementing this algorithm such as training a single FNN for all different speeds and friction levels.

Conclusion

This paper has shown that the friction coefficient can be estimated to within an average MAE of 0.0083 using wheelset acceleration measurements and FNNs. Unlike existing methods, the FNN estimator does not depend on slip velocities that are difficult to obtain, subject to drift, inherent sensitivities in the slip/adhesion curve, or other vehicle/creep force model parameters, or model-based force estimation that is subject to error due to linear estimates of suspension parameters. Instead, the FNN relies only on the longitudinal accelerations data of the wheelsets that are HP and LP filtered. It consists of only a single hidden layer with six neurons and uses hyperbolic tangent and logsig functions for its hidden and output layer for PR. The FNNs' estimation performance has been validated by the data obtained from a full-size two-car rail vehicle running on tacks with 5 different modified and measured friction conditions. To the authors knowledge, this is the first time wheelset measurements from full-size vehicle without braking have been used for directly estimating the friction or adhesion coefficient at different friction conditions. It does not require high computational time so that, if implemented, it can immediately inform drivers about low adhesion conditions, which could be used to slow down the vehicle earlier since low adhesion conditions can extend for some period in some cases, e.g. leaves on the rails for a long section of the track.

As with any NN estimator it will only be accurate if it is implemented around the speed and friction conditions that are used in the training. The current results represent a proof-of-concept, but if implemented for a specific vehicle the method would require re-training to match the capabilities of the vehicle. The results span a range of friction conditions as would be experienced by a vehicle in service. However, sustained very low friction (< 0.05) was challenging to create during the test programme so this could be an area in which additional training of the model would be required. Alternatively, it might be considered that anything less than 0.1 represents an emergency condition below which detailed measurement no longer aids operation. One of the future tasks is to train five different FNNs for five different friction conditions that creates a variation in the vehicle speed, which can show an indication of the performance of the FNN friction estimation at varying speeds.

Acknowledgements

This paper is part of a project on creating an onboard rail-wheel friction measuring capability for continuous data collection under normal operating conditions, and the authors are grateful to Elaine Cockroft, Mark Burstow and Simon Chaney from Network Rail for their contributions to smooth running of the project, Kartik Chandrasekhar and David Vincet from Hitachi Rail UK for fully instrumenting the test vehicle, and Stuart Brown at DB ESG, UK for assistance with paper tape application.

Disclosure statement

No potential conflict of interest was reported by the author(s).

Funding

This research was funded by Network Rail, UK.

ORCID

Peter Hubbard http://orcid.org/0000-0003-2730-2538

References

[1] Rowell B, Richardson W. An assessment of the available adhesion and slip risk for ERTMS. London: RSSB; 2003.
[2] RSSB. (2023). Adhesion.: Accessed: 07/03/2023. Available at: https://www.rssb.co.uk/en/what-we-do/key-industry-topics/adhesion.
[3] Spiryagin M, Cole C, Sun YQ, et al. General modelling techniques. Design and simulation of rail vehicles. Boca Raton (Florida): CRC Press/Taylor and Francis; 2014. P. 79–95.
[4] Olofsson U. Adhesion and friction modification. Wheel–rail interface handbook. Cambridge: Woodhead Publishing; 2009. p. 510–527.
[5] Shrestha S, Wu Q, Spiryagin M. Review of adhesion estimation approaches for rail vehicles. Int J Rail Transport. 2019;7(2):79–102. doi:10.1080/23248378.2018.1513344
[6] Chen B, Huang Z, Liu W, et al. A Novel Adhesion Force Estimation for Railway Vehicles Using an Extended State Observer," *IECON 2019 – 45th Annual Conference of the IEEE Industrial Electronics Society, Lisbon, Portugal*, 2019. p. 225–230. doi:10.1109/IECON.2019.8926857
[7] Olofsson U, Lewis R. Tribology of the wheel-rail contact. In: Iwnicki S, editor. Handbook of railway vehicle dynamics. Boca Raton, FL: CRC Press; 2006. p. 121–138.
[8] Lyu Y, Bergseth E, Olofsson U. Open system tribology and influence of weather condition. Sci Rep. 2016;6:32455.
[9] Chen H, Tanimoto H. Experimental observation of temperature and surface roughness effects on wheel/rail adhesion in wet conditions. Int J Rail Transport. 2018;6:101–112.
[10] Gajdar T, Rudas I, Suda Y. (1997). Neural network based estimation of friction coefficient of wheel and rail. *IEEE International Conference on Intelligent Engineering Systems*; Sep, Budapest, Hungary. p. 315–318.
[11] Chen H, Ishida M, Namura A, et al. Estimation of wheel/rail adhesion coefficient under wet condition with measured boundary friction coefficient and real contact area. Wear. 2011;271(1–2):32–39. doi:10.1016/j.wear.2010.10.022

[12] Kim MS. Study on the adhesion characteristic between wheel and rail using the scaled testbench. Int J Mech. 2015;9:198–205.
[13] Gallardo-Hernandez EA, Lewis R. Twin disc assessment of wheel/rail adhesion. Wear. 2008;265:1309–1316.
[14] Fletcher DI, Lewis S. Creep curve measurement to support wear and adhesion modelling: using a continuously variable creep twin disc machine. Wear. 2013;298–299(1):57–65. doi:10.1016/j.wear.2012.11.065
[15] Fletcher DI. A new two-dimensional model of rolling-sliding contact creep curves for a range of lubrication types. Proc Inst Mech Eng Part J – J Eng Tribol. 2013;227(J6):529–537. doi:10.1177/1350650112465694
[16] Bosso N, Zampieri N. Experimental and numerical simulation of wheel-rail adhesion and wear using a scaled roller rig and a real-time contact code. Shock Vib. 2014;2014:1–14.
[17] Bosso N, et al. (2009). Methodology for the determination of wheel-roller friction coefficient on 1/5 scaled test rig. 8th Intern. Con. on Contact Mechanics and wear of Rail/Wheel Syst. Firenze, Italy.
[18] Charles G, Goodall RM. Low adhesion estimation. The Institution of Engineering and Technology International Conference on Railway Condition Monitoring; 2006 Nov, Birmingham, UK. pp. 96–101.
[19] Charles G, Goodall R, Dixon R. Model-based condition monitoring at the wheel–rail interface. Vehicle Syst Dyn. 2008;46:415–430.
[20] Lewis R, Trummer G, Six K, et al. Leaves on the line: characterising leaf based low adhesion on railway rails. Tribol Int. 2023;185:108529.
[21] Allotta B, Meli E, Ridolfi A, et al. Development of an innovative wheel–rail contact model for the analysis of degraded adhesion in railway systems. Tribol Int. 2014;69:128–140. doi:10.1016/j.triboint.2013.09.013
[22] Xia F, Cole C, Wolfs P. Grey box-based inverse wagon model to predict wheel–rail contact forces from measured wagon body responses. Vehicle Syst Dyn. 2008;46:469–479.
[23] Xia F, Cole C, Wolfs PJ. (2008). Wheel rail contact forces prediction and validation with field tests. *Conference on Railway Engineering (CORE2008), Perth, Australia*. p. 73–82.
[24] Pichlik P, Zdenek J. Extended Kalman filter utilization for a railway traction vehicle slip control. 2017 International Conference on Optimization of Electrical and Electronic Equipment (OPTIM) & 2017 Intl Aegean Conference on Electrical Machines and Power Electronics (ACEMP); 2017 May, Brasov, Romania: IEEE; p. 869–874.
[25] Zhao Y, Liang B, Iwnicki S. Friction coefficient estimation using an unscented Kalman filter. Vehicle Syst Dyn. 2014;52:220–234.
[26] Zhao Y, Shen L, Jiang Z, et al. Real-time wheel–rail friction coefficient estimation and its application. Veh Syst Dyn. 2023. doi:10.1080/00423114.2022.2159846
[27] Onat A, Voltr P, Lata M. A new friction condition identification approach for wheel–rail interface. Int J Rail Transportation. 2017;5:127–144.
[28] Ward CP, Goodall RM, Dixon R, et al. Adhesion estimation at the wheel–rail interface using advanced model-based filtering. Vehicle Syst Dyn. 2012;50:1797–1816.
[29] Hubbard PD, Ward C, Dixon R, et al. Models for estimation of creep forces in the wheel/rail contact under varying adhesion levels. Vehicle Syst Dyn. 2014;52:370–386.
[30] Hubbard PD, Amarantidis GA, Ward CP. Leaves on the line: low adhesion detection in railways. IFAC-PapersOnLine. 2016;49(21):467–472.
[31] Ward C, Goodall RM, Dixon R. (2011). Creep force estimation at the wheel-rail interface. *22nd International Symposium on Dynamics of Vehicles on Roads and Tracks; Aug: Manchester, UK*. p. 1–6.
[32] Ward CP, Goodall RM, Dixon R. Contact Force Estimation in the Railway Vehicle Wheel Rail Interface. *18th International Federation of Automatic Control (IFAC); 2011 Jan, Milano, Italy*. p. 4398–4403.
[33] Hubbard PD, Ward C, Dixon R, et al. Verification of model-based adhesion estimation in the wheel-rail interface. Chem Eng Trans. 2013;33:757–762.

[34] Hubbard PD, Ward C, Goodall RM, et al. Real time detection of low adhesion in the wheel/rail contact. *RRUKA Annual Conference; 2012, London, UK*; p. 1–5.
[35] Hussain I, Mei TX, Ritchings RT. Estimation of wheel–rail contact conditions and adhesion using the multiple model approach. Vehicle Syst Dyn. 2013;51:32–53.
[36] Strano S, Terzo M. On the real-time estimation of the wheel-rail contact force by means of a new nonlinear estimator design model. Mech Syst Signal Process. 2018;105:391–403. doi:10.1016/j.ymssp.2017.12.024
[37] Spiryagin M, Cole C, Sun YQ. Adhesion estimation and its implementation for traction control of locomotives. Int J Rail Transp. 2014;2(3):187–204.
[38] Shrestha S, Spiryagin M, Wu Q. Friction condition characterization for rail vehicle advanced braking system. Mech Syst Signal Process. 2019;134(106324).
[39] Urda P, Aceituno JF, Muñoz S, et al. Artificial neural networks applied to the measurement of lateral wheel-rail contact force: A comparison with a harmonic cancellation method. Mech Mach Theory. 2020;153; doi:10.1016/j.mechmachtheory.2020.103968
[40] Falomi S, Malvezzi M, Meli E, et al. Determination of wheel-rail contact points: comparison between classical and neural network based procedures. Meccanica. 2009;44:661–686. doi:10.1007/s11012-009-9202-6
[41] Escalona JL, Aceituno JF. Multibody simulation of railway vehicles with contact lookup tables. Int J Mech Sci. 2019;155:571–582. doi:10.1016/j.ijmecsci.2018.01.020
[42] Malvezzi M, Pugi L, Papini S, et al. Identification of a wheel–rail adhesion coefficient from experimental data during braking tests. Proc Inst Mech Eng Part F: J Rail Rapid Transit. 2013;227:128–139.
[43] Liu J, Liu L, He J, et al. Wheel/rail adhesion state identification of heavy-haul locomotive based on particle swarm optimization and kernel extreme learning machine. J Adv Transport. 2020;2020:1–6.
[44] Zirek A, Onat A. A novel anti-slip control approach for railway vehicles with traction based on adhesion estimation with swarm intelligence. Rail Eng Sci. 2020;28:346–364. doi:10.1007/s40534-020-00223-w
[45] Iwnicki S. Handbook of railway vehicle dynamics. Boca Raton: CRC/Taylor & Francis; 2006.
[46] Mickoski H, Djidrov M, Mickoski I. Estimation and analysis of various influential factors in the braking process of rail vehicles. Veh Syst Dyn. 2021;59(1):1–16.
[47] Network Rail. Tuxford Rail Innovation & Development Centre, https://www.networkrail.co.uk/industry-and-commercial/research-development-and-technology/rail-innovation-development-centres/tuxford-rail-innovation-development-centre/, Accessed 2023/06/21.
[48] Fulford C. "Review of Low Adhesion Research," RSSB, London, 2004.
[49] Watson M, Whire B, Lanigan J, et al. The composition and friction-reducing properties of leaf layers: leaf layer friction and composition. Proc R Soc Lond A Math Phys Sci. 2020;476(2239):1–14.
[50] Lewis R, Lewis SR, Zhu Y, et al. The modification of a slip resistance meter for measurement of railhead adhesion. Proc Inst Mech Eng Part F J Rail Rapid Transit. 2012;227(2):196–200.
[51] Eadie DT, Harrison H, Kempka R, et al. "Field assessment of friction and creepage with a new tribometer," in *Proc. 11th Int. Conf. Contact Mech. Wear Rail/wheel Syst. C.*, 2018.
[52] White B, Lewis R, Fletcher D, et al. Rail-wheel friction quantification and its variability under lab and field trial conditions. Proc Inst Mech Eng Part F: J Rail Rapid Transit. 2023;0(0). doi:10.1177/09544097231209483
[53] Pugi L, Paolieri G, Giorgetti M, et al. Bocciolini HIL testing of wheel slide protection systems: criteria for continuous updating and validation (2023). Railway Eng Sci; 31(2):108–121. doi:10.1007/s40534-022-00298-7
[54] Harrison T, Abduraxman B, Hubbard P, et al. Creation of and measurement of Low Adhesion Conditions for the development of on-train Low Adhesion Detection equipment', International Association for Vehicle System Dynamics Symposium, Ottawa, Canada, August 2023.